Effect of inertia on double diffusive bidispersive convection

B. Straughan
Department of Mathematics
University of Durham, DH1 3LE, U.K.

September 3, 2018

Abstract

Convection thresholds in a saturated bidisperse porous material are calculated in the presence of a non-zero coefficient of inertia, the acceleration coefficient, for the fluid velocity in the macro pores. We concentrate on the case where the layer is heated from below and simultaneously salted from below. The effect of increasing the size of the acceleration coefficient is generally to increase the critical Rayleigh number above which convective motion commences, although the precise values depend on the interaction coefficient between the micro and macro pores, the porosities, and the Lewis number.

1 Introduction

Thermal convection in a double porosity material is a topic of increasing research interest. Double porosity materials are also known as bidispersive media and, in addition to possessing the usual macro porosity well known in porous media theory, there are cracks or fissures in the porous skeleton which give rise to a micro porosity. Bidispersive porous materials may also be constructed in a laboratory, as indicated by Nield & Kuznetsov [1]. The topic of heat and mass transfer in a bidisperse porous material has created interest in the chemical engineering literature for quite a while, as witnessed by the work of Burghardt *et al.* [2], Szczygiel [3, 4] and Valus & Schneider [5]. A major reason why heat and mass transfer in bidisperse porous media theory is of interest is the discovery that these effects are very important in many real engineering and geophysical applications. The book by Straughan [6] discusses several of these applications, but it is cogent to mention some particular ones at this juncture. For example, biporous media feature in wicks in heat pipes, see e.g. Lin *et al.* [7], Mottet & Prat [8], Taqvi *et al.* [9], Yeh *et al.* [10]. Application of bidisperse porous media theory to the mundane but extremely important area of landslides is another diverse area, see e.g. Borja *et al.* [11], Borja & White [12], Montrasio *et al.* [13], and Scotto di Santolo & Evangelista [14]. We finally mention stockpiling

of coal where relatively small pieces of coal are stockpiled but the individual pieces contain cracks or small pores. Piles of coal may self combust and so an understanding of heat transfer in this case is vital, see Hooman & Maas [15], Hooman *et al.* [16].

In this paper our interest is in double diffusive convection, or thermosolutal convection, in a bidisperse porous body. This involves heat transfer in a bidisperse porous medium when the saturating fluid also contains a concentration of dissolved salt. In the case of a single porosity body thermosolutal convection was first described and the analysis resolved in the fundamental article of Nield [17]. Since then, many articles have appeared in the single porosity case, also dealing with nonlinear stability, see e.g. Barletta & Nield [18], Deepika [19], Deepika & Narayana [20], Harfash [21], Harfash & Hill [22], Hill & Morad [23], Love *et al.* [24], Mulone [25], Simmons *et al.* [26], Straughan [27, 28, 29]. A theory of and analysis for double diffusive convection in a bidisperse porous material was presented by Straughan [30], who neglected inertia in the fluid in both the macro and micro phases.

Nield & Bejan [31] devote much of section 1.5 of their book to models which incorporate inertia. In a single porosity medium the momentum equation is given by, Nield & Bejan [31],

$$\rho c_a \frac{\partial v_i}{\partial t} + \frac{\rho c_F}{\sqrt{K}} |\mathbf{v}| v_i = -p_{,i} - \frac{\mu}{K} v_i, \tag{1}$$

where ρ is fluid density, v_i velocity, K is permeability, p pressure, μ dynamic viscosity, c_a is the acceleration coefficient and c_F is a dimensionless form drag coefficient. As Nield & Bejan [31] point out, c_a may in general be a tensor, but we restrict attention to the isotropic case. The second term in (1) is the Forchheimer term and the effect of this upon convection is analysed by Rees [32, 33]. In this paper we neglect the Forchheimer term as we are not considering high flow rates, but we do retain a term like the c_a one in (1), but only for the macro velocity in a bidisperse porous medium.

For a single porosity medium the effect of the c_a term upon the critical Rayleigh number for thermal convection has been studied by several writers. Vadasz [34] discovered this term has a striking effect on rotating porous convection. Other interesting studies include Altawallbeh *et al.* [35], Bhadauria & Srivastava [36], Deepika [19], Falsaperla *et al.* [37], Harfash & Challoob [38], Straughan [39, 40, 41]. As far as we are aware, this is the first study of inertia effects via an acceleration coefficient, on convection in a bidisperse porous medium.

The theory of thermal convection in a bidisperse porous medium was presented in fundamental work by Nield & Kuznetsov [42, 1, 43, 44, 45] and by Nield [46]. Falsaperla *et al.* [47] and Gentile & Straughan [48] continued the work of Nield & Kuznetsov but they restrict attention to a single temperature field which still has many real applications. Other recent papers dealing with the single temperature field model are by Franchi *et al.* [49], Gentile & Straughan [50], and Straughan [51, 30].

The aim of this paper is to generalize the work of Straughan [30] on double diffusive bidispersive convection but consider the effect of a non-zero inertia term in the macro fluid velocity equation. We restrict attention to the more mathematically difficult but contemporarily more physically interesting case where the layer is heated from below and simultaneously salted from below. In this situation the heating wishes to destabilize the layer and initiate convective overturning whereas the salt gradient acts in the opposite manner and is stabilizing. The inertia term will be seen to have a very strong effect on the convection thresholds and we believe this is a justification for the analysis.

2 Equations

The governing equations change very little from those given by Straughan [30]. Indeed, the only difference is in the inclusion of an acceleration term in equation $(1)_1$ of Straughan [30]. Thus, equation $(1)_1$ of Straughan [30] is replaced by

$$\rho_0 c_a \frac{\partial U_i^f}{\partial t} = -\frac{\mu}{K_f} U_i^f - p_{,i}^f - \zeta(U_i^f - U_i^p) + g\rho_0 \alpha k_i T - \alpha_C \rho_0 g k_i C, \qquad (2)$$

where ρ_0 is the fluid density, c_a is the acceleration coefficient, U_i^f and U_i^p are the fluid velocities in the macro and micropores, K_f is the permeability in the macro phase, ζ is the coefficient of momentum transfer betwen the macro and micro phases as defined by Nield & Kuznetsov [1], g is gravity, α thermal expansion coefficient, T temperature, C salt concentration and α_C is the coefficient in the equation of state for the basic density ρ, namely

$$\rho = \rho_0 \big[1 - \alpha(T - T_0) + \alpha_C (C - C_0)\big].$$

All other notation and equations are exactly as in Straughan [30], section 2.

We are interested in investigating thermosolutal convection in a plane layer of bidispersive material. As in Straughan [30], the saturated porous material occupies the horizontal layer $0 < z < d$, $\{(x, y) \in \mathbb{R}^2\}$, and the equations are (2) of this paper coupled with equations $(1)_{2,3,4}$, (2) and (5) of Straughan [30]. The basic solution and non-dimensionalization is exactly the same as in section 3 of Straughan [30]. The perturbation equations may be found as equations (12) of Straughan [30] allowing for the addition of the $\rho_0 c_a$ term in (2) and omitting the Soret effect. For completeness, we record the non-dimensional perturbation equations here, namely,

$$\begin{aligned}
&- J u_{i,t}^f - u_i^f - \xi(u_i^f - u_i^p) - \pi_{,i}^f + R\theta k_i - \mathcal{C}\gamma k_i = 0\,,\\
&u_{i,i}^f = 0\,,\\
&- K^r u_i^p - \xi(u_i^p - u_i^f) - \pi_{,i}^p + R\theta k_i - \mathcal{C}\gamma k_i = 0\,,\\
&u_{i,i}^p = 0\,,\\
&\theta_{,t} + (u_i^f + u_i^p)\theta_{,i} = w^f + w^p + \Delta\theta\,,\\
&\epsilon_1 Le\gamma_{,t} + ALe(u_i^f + u_i^p)\gamma_{,i} = (w^f + w^p) + \Delta\gamma\,,
\end{aligned} \qquad (3)$$

where J is a non-dimensional form of the acceleration coefficient.

Equations (3) hold in the domain $\{(x,y)\in\mathbb{R}^2\}\times\{z\in(0,1)\}\times\{t>0\}$ and with $\mathbf{u}^f=(u^f,v^f,w^f)$, $\mathbf{u}^p=(u^p,v^p,w^p)$. The boundary conditions become

$$w^f=0,\, w^p=0,\, \theta=0,\, \gamma=0, \qquad z=0,d, \tag{4}$$

and the perturbation solution satisfies a plane tiling planform in the horizontal directions with wavenumber a. In particular, we observe that R is the Rayleigh number and $\mathcal{C}$ is the concentration Rayleigh number given by equations (11) of Straughan [30].

3 Instability

To analyse instability for (3) and (4) we take curl curl of $(3)_{1,3}$ and retain the w_f and w^p components of the results. Equations $(3)_5$ and $(3)_6$ are linearized and then a time dependence like $e^{\sigma t}$ is requested. This results in having to solve the eigenvalue problem for the boundary conditions (4) together with the equations

$$\begin{aligned}
&(1+\xi+J\sigma)\Delta w^f-\xi\Delta w^p-R\Delta^*\theta+\mathcal{C}\Delta^*\gamma=0\,,\\
&(K^r+\xi)\Delta w^p-\xi\Delta w^f-R\Delta^*\theta+\mathcal{C}\Delta^*\gamma=0\,,\\
&\sigma\theta=w^f+w^p+\Delta\theta\,,\\
&\epsilon_1 Le\sigma\gamma=w^f+w^p+\Delta\gamma\,,
\end{aligned} \tag{5}$$

where $\Delta^*=\partial^2/\partial x^2+\partial^2/\partial y^2$ is the horizontal Laplacian.

To solve (5) we follow the method of Chandrasekhar [52] and employ a normal mode representation and set $w^f=W^f(z)f(x,y)$ with similar forms for w^p,θ and γ. This results in solving the determinant equation

$$\begin{vmatrix}
-(1+\xi+J\sigma)\Lambda & \xi\Lambda & Ra^2 & -\mathcal{C}a^2\\
\xi\Lambda & -(K^r+\xi)\Lambda & Ra^2 & -\mathcal{C}a^2\\
1 & 1 & -(\Lambda+\sigma) & 0\\
1 & 1 & 0 & -(\Lambda+\mathcal{L}\sigma)
\end{vmatrix}=0 \tag{6}$$

where $\Lambda=n^2\pi^2+a^2$ and $\mathcal{L}=\epsilon_1 Le$. The number n arises from the representation of $W^f=\hat{W}^f\sin n\pi z$ and a is the wavenumber.

Upon expansion this determinant yields the equation

$$\begin{aligned}
Ra^2\big[\Lambda A+\mathcal{L}J\sigma^2+\sigma\{\mathcal{L}A+J\Lambda\}\big]&=\mathcal{C}a^2\big[\Lambda A+J\sigma^2+\sigma\{A+J\Lambda\}\big]\\
&+\Lambda\big[\Lambda^2B+\sigma\{\Lambda^2JD+\Lambda(1+\mathcal{L})B\}\\
&\quad+\sigma^2\{\mathcal{L}B+\Lambda(1+\mathcal{L})JD\}+\mathcal{L}JD\sigma^3\big],
\end{aligned} \tag{7}$$

where we have put

$$A=1+4\xi+K^r, \qquad B=K^r+\xi K^r+\xi, \qquad D=K^r+\xi.$$

The stationary convection boundary, $\sigma = 0$, follows quickly from (7) which in that case becomes

$$R = \mathcal{C} + \frac{\Lambda^2}{a^2}\frac{B}{A}.$$

Upon minimizing in n^2 and then in a^2 one finds the critical wavenumber is $a^2 = \pi^2$ and then the stationary convection curve is

$$R = \mathcal{C} + 4\pi^2\frac{B}{A}\,. \tag{8}$$

To find the oscillatory convection boundary we put $\sigma = i\sigma_1$, $\sigma_1 \in \mathbb{R}$, cf. Chandrasekhar [52]. Then, take the real and imaginary parts of (7) to obtain the following two equations

$$\begin{aligned} Ra^2[\Lambda A - \sigma_1^2 J\mathcal{L}] &= \mathcal{C}a^2[\Lambda A - J\sigma_1^2] \\ &\quad + B\Lambda^3 - \sigma_1^2\Lambda\big[\mathcal{L}B + J\Lambda(1+\mathcal{L})D\big], \end{aligned} \tag{9}$$

and

$$\begin{aligned} Ra^2[J\Lambda + \mathcal{L}A] &= \mathcal{C}a^2[J\Lambda + A] \\ &\quad + (1+\mathcal{L})\Lambda^2 B + J\Lambda^3 D - \sigma_1^2 J\mathcal{L}\Lambda D. \end{aligned} \tag{10}$$

These equations then yield σ_1^2 as

$$\sigma_1^2 = -RE + F, \tag{11}$$

where

$$E = a^2\Big(\frac{1}{\mathcal{L}D} + \frac{A}{JD\Lambda}\Big)$$

and

$$F = \mathcal{C}a^2\Big(\frac{1}{\mathcal{L}D} + \frac{A}{J\mathcal{L}D\Lambda}\Big) + \frac{(1+\mathcal{L})B\Lambda}{J\mathcal{L}D} + \frac{\Lambda^2}{\mathcal{L}}\,.$$

Expression (11) may then be employed in (9) to yield the following form for R,

$$XR^2 - YR + Z = 0, \tag{12}$$

where

$$\begin{aligned} X &= a^2 J\mathcal{L}E, \\ Y &= \mathcal{C}a^2 JE + J\mathcal{L}Fa^2 + EH - a^2 A\Lambda, \\ Z &= HF + \mathcal{C}a^2 JF - B\Lambda^3 - \mathcal{C}a^2 A\Lambda. \end{aligned}$$

One may show $Y > 0$ and then R is found as

$$R = \frac{Y - \sqrt{Y^2 - 4XZ}}{2X}\,. \tag{13}$$

The critical value of R is found from (13) numerically by minimizing in a^2 and n^2. We check numerically that $Y^2 > 4XZ$, and this is so for all values presented here. For all the computations displayed here we found that $n = 1$ yields the minimum. Once the critical wavenumber is found from (13), i.e. that value which yields a minimum for R, equation (11) leads to the equivalent value for σ_1^2.

4 Numerical results and conclusions

In this section we report on numerical solutions for the critical Rayleigh number and wavenumber thresholds, based on (8) for the stationary convection case, and by minimizing (13) in a^2 for the oscillatory convection scenario.

We focus on the case where the saturating fluid is water and the porous medium is sand. We take the macro porosity ϕ to have value 0.3 whereas the micro porosity ϵ has value 0.2. The value of $\mathcal{L} = \epsilon_1 Le$ is 55.924, cf. Straughan [30].

The parameters ξ and K^r are varied and we report on cases where $\xi = 0.1$ and 0.5, and $K^r = 1.5$ and 5.

Figure 1 shows a typical instability threshold curve, in this case $\xi = 0.1, K^r = 1.5$ and the inertia coefficient $J = 0.8$. For $0 \leq \mathcal{C} \leq 4.22$ we see that instability arises by stationary convection, represented by the straight line in figure 1 emanating from the $\mathcal{C} = 0$ value where R is less than 24. At the transition point $C^* = 4.22$ the mechanism of instability switches to oscillatory convection for $\mathcal{C} > C^*$ and the curve which branches from $(R, \mathcal{C}) = (28.04, 4.22)$ to the right represents the oscillatory curve threshold. In our graphs oscillatory curves appear to be straight lines although they are not, a fact pointed out in the single porosity case by Straughan [28]. The point is they arise from (13) which does not lead to a straight line. For all of the values of ξ, K^r and J we tried, figure 1 displays the typical shape, although the quantitative values of R and $\mathcal{C}$ change depending on ξ, K^r and J.

Figure 2 displays the stationary convection and oscillatory curves when $J = 0.1, 0.3, 0.5, 0.8$ and 1.0, with $\xi = 0.1$ and $K_r = 1.5$. The transition values from stationary to oscillatory convection are given in tabular form in table 1, for $J = 0.1, 0.3, 0.5, 0.8$ and 1.0. The corresponding critical wavenumber values are likewise displayed in table 1. In addition, the values of σ_1^2 are given in table 1, where R denotes the oscillatory convection value whereas R_{stat} denotes the stationary convection value. It is noteworthy that as J increases σ_1^2 is not zero at the transition (the negative value for $J = 0.1$ is purely indicative of stationary convection and arises from equation (11)). Table 4 confirms this phenomenon. The last effect was also observed in the single porosity case by Straughan [28].

The analogous curves to those of figure 2 are given in figures 3, 4 and 5 when $K_r = 5, \xi = 0.1$, $K_r = 1.5, \xi = 0.5$, and $K_r = 5, \xi = 0.5$, respectively. In each case the inertia coefficient takes the values $J = 0.1, 0.3, 0.5, 0.8$ and 1.0. The corresponding values at the transition from stationary to oscillatory convection are given in tables 2 - 4.

What is evident from figures 2 - 5 is that is we fix K_r and vary ξ then the critical Rayleigh numbers change by a relatively small amount. However, when we fix ξ and vary K_r then the variation in critical Rayleigh numbers is greater. In all cases increasing the inertia coefficient leads to increasing critical Rayleigh numbers and increasing transition values. This, for insulation, where no convection is desired to decrease heat transfer, one requires as small an inertia as possible. On the other hand, if one desires efficient heat transfer, then a greater inertia coefficient is preferable. This highlights the need for accurate

measurements of the quantities involved in the non-dimensional numbers ξ, K_r and J.

We include one graph of the critical wavenumber variation, in figure 6, for $\xi = 0.5$ and $K_r = 1.5$, corresponding to figure 4. The variation in J is not huge, but we see that oscillatory convection lowers the wave number as $\mathcal{C}$ and J increase. This means that the convection cell aspect ratio decreases and the cells become wider. For each value of J the stationary convection wavenumber is constant with value $a^2 = \pi^2 \approx 9.8696$. For a particular value of J when $\mathcal{C}$ increases to the transition value C^* the wavenumber jumps from π^2 to the value shown on the oscillatory convection curves. In each case the cell becomes wider since a^2 decreases discontinuously. The transition values are $J = 0.1, R = 24.996, C^* = 0.87, a^2 = 9.7032$; $J = 0.3, R = 25.856, C^* = 1.73, a^2 = 9.4117$; $J = 0.5, R = 26.710, C^* = 2.58, a^2 = 9.1659$; $J = 0.8, R = 27.966, C^* = 3.84, a^2 = 8.8603$; $J = 1.0, R = 28.796, C^* = 4.67, a^2 = 8.6885$.

A referee raised the issue of producing graphs for the variation of R in ξ and in K_r. This is an interesting question but there are four parameters, ξ, K_r, J and $\mathcal{C}$ and the graphs depend on all four.

When the convection is stationary then from (8) we find $\partial R/\partial K_r = 4\pi^2(1+2\xi)^2/A^2 > 0$ and $\partial R/\partial \xi = 4\pi^2(1-K_r)^2/A^2$, and so R increases with increasing K_r and ξ, keeping the other parameters fixed. For example, in figures 2 and 3, if $\mathcal{C} = 0.5$ we see stationary convection for all $J = 0.1, 0.3, 0.5, 0.8$ and 1.0 with R increasing in K_r. When $\mathcal{C} = 3.5$ there is a transition from stationary to oscillatory convection for $J = 0.1, 0.3, 0.5$, as $\mathcal{C}$ increases for $K_r = 1.5$ and likewise for $J = 0.1, 0.3$, for $K_r = 5.0$. When $\mathcal{C} = 10$ all curves exhibit the stationary to oscillatory transition for $J = 0.1, 0.3, 0.5, 0.8$ and 1.0 and for $K_r = 1.5$ and 5. However, R is always increasing in K_r. The increase in ξ is less prominent. We refrain from producing graphical output for K_r and ξ varying since $K_r = K^f/K^p$ and $\xi = \zeta K^f/\mu$. Experimental values for the micro permeability, K^p, and the coefficient of momentum transfer between the macro and micro phases, ζ, do not appear to be readily available. There is thus a need for such values for real materials and if available graphical output could be readily produced.

In this article we concentrate on the case where the layer is heated from below and salted from below. It is worth pointing out that if one considers the analogous problem with inertia when the layer is heated from below and salted from above then one may show that the linear instability boundary is identifiable to the global nonlinear stability boundary. Thus, in that case one achieves an optimal result by finding linear instability thresholds.

We have only considered the case of flow in the macro pores and micro pores when the porous material is of Darcy type. The analogous class of problem when one employs a Brinkman theory may lead to very different results. Straughan [53] has shown in the case of a single porosity material that completely different qualitative and quantitative behaviour may be found in the same problem depending on whether one employs Darcy or Brinkman theory. Furthermore, we only employ Fourier's law relating the heat flux to the temperature gradient. If one were to employ a hyperbolic law such as one of Cattaneo-Christov type

then even for Darcy theory the behaviour may change significantly, as observed by Straughan [54] when dealing with a single porosity model.

Acknowledgments.

I am indebted to three anonymous referees whose incisive comments have led to improvements in the original manuscript.

References

[1] Nield, D.A. and Kuznetsov, A.V. The onset of convection in a bidisperse porous medium. Int. J. Heat Mass Transfer, 49 (2006) 3068-3074.

[2] Burghardt, A., Rogut, J. and Gotkowska, J. Diffusion coefficients in bidisperse porous structures, Chemical Engng. Science, 43 (1988) 2463–2476.

[3] Szczygiel, J. Enhancement of reforming efficiency by optimising the porous structure of reforming catalyst: theoretical considerations, Fuel, 85 (2006), 1579–1590.

[4] Szczygiel, J. Control of transport phenomena in the interior of the reforming catalyst grain: a new approach to the optimisation of the reforming process, Fuel Processing Technology, 92 (2011), 1434–1448.

[5] Valus, J. and Schneider, P. Transport characteristics of bidisperse porous $\alpha-$ aluminas, Applied Catalysis, 16 (1985), 329–341.

[6] Straughan, B. Mathematical aspects of multi-porosity continua, volume 38 of Adv. Mechanics and Mathematics, Springer, Cham, Switzerland, 2017.

[7] Lin, F.C., Liu, B.H., Huang, C.T. and Chen, Y.M. Evaporative heat transfer model of a loop heat pipe with bidisperse wick structure. Int. J. Heat Mass Transfer 54 (2011), 4621–4629.

[8] Mottet, L. and Prat, M. Numerical simulation of heat and mass transfer in bidispersed capillary structures: application to the evaporator of a loop heat pipe. Applied Thermal Engineering 102 (2016), 770–784.

[9] Taqvi, S.M., Vishnoi, A. and Levan, M.D. Effect of macropore convection on mass transfer in a bidisperse adsorbent particle. Adsorption 3 (1997), 127–136.

[10] Yeh, C.C., Chen, C.N. and Chen, Y.M. Heat transfer analysis of a loop heat pipe with biporous wicks. Int. J. Heat Mass Transfer 52 (2009), 4426–4434.

[11] Borja, R. L., Liu, X. and White, J. A., Multiphysics hillslope processes triggering landslides, Acta Geotechnica, 7 (2012), 261–269.

[12] Borja, R. L. and White, J. A., Continuum deformation and stability analyses of a steep hillside slope under rainfall infiltration, Acta Geotechnica, 5 (2010), 1–14.

[13] Montrasio, L., Valentino, R. and Losi, G. L., Rainfall infiltration in a shallow soil: a numerical simulation of the double - porosity effect, Electronic J. Geotechnical Engineering, 16 (2011), 1387–1403.

[14] Scotto di Santolo, A. and Evangelista, A., Calibration of a rheological model for debris flow hazard mitigation in the Campania region, in "Landslides and engineered slopes. From the past to the future", eds. Chen, Z., Zhang, J. M., Ho, K., Wu, F. Q. and Li, Z. K. Taylor and Francis, London, pp. 913–919, (2008).

[15] Hooman, K. and Maas, U. Theoretical analysis of coal stockpile self-heating. Fire Safety J. 67 (2014), 107–112.

[16] Hooman, K., Sauret, E. and Dahari, M. Theoretical modelling of momentum transfer function of bi-disperse porous media. Applied Thermal Engineering 75 (2015), 867–870.

[17] Nield, D.A. Onset of thermohaline convection in a porous medium. Water Resources Research 4 (1968), 553–560.

[18] Barletta, A. and Nield, D.A. Thermosolutal convective instability and viscous dissipation effect in a fluid-saturated porous medium. Int. J. Heat Mass Transfer 54 (2011), 1641–1648.

[19] Deepika, N. Linear and nonlinear stability of double-diffusive convection with the Soret effect. Transport in Porous Media 121 (2018), 93–108.

[20] Deepika, N. and Narayana, P.A.L. Nonlinear stability of double-diffusive convection in a porous layer with throughflow and concentration based internal heat source. Transport in Porous Media 111 (2016), 751–762.

[21] Harfash, A.J. Three-dimensional simulations for convection problems in anisotropic porous media with nonhomogeneous porosity, thermal diffusivity, and variable gravity effects. Transport in Porous Media 102 (2014), 43–57.

[22] Harfash, A.J. and Hill, A.A. Simulation of three-dimensional double-diffusive throughflow in internally heated anisotropic porous media. Int. J. Heat Mass Transfer 72 (2014), 609–615.

[23] Hill, A.A. and Morad, M.R. Convective stability of carbon sequestration in anisotropic porous media. Proc. Roy. Soc. London A 470 (2014), 20140373.

[24] Love, A.J., Simmons, C.T. and Nield, D.A. Double-diffusive convection in groundwater wells. Water Resources Research 43 (2007), W08428.

[25] Mulone, G. On the nonlinear stability of a fluid layer of a mixture heated and salted from below. Continuum Mech. Thermodyn. 6 (1994), 161–184.

[26] Simmons, C.T., Sharp, J.M. and Nield, D.A. Models of free convection in fractured low-permeability media. Water Resources Research 44 (2008), W03431.

[27] Straughan, B. Stability and wave motion in porous media, volume 165 of Applied Mathematical Sciences, Springer, New York, 2008.

[28] Straughan, B. Anisotropic inertia effect in microfluidic porous thermosolutal convection. Microfluidics and Nanofluidics 16 (2014), 361–368.

[29] Straughan, B. Convection with local thermal non-equilibrium and microfluidic effects, volume 32 of Adv. Mechanics and Mathematics, Springer, Cham, Switzerland, 2015.

[30] Straughan, B. Bidispersive double diffusive convection. Int. J. Heat Mass Transfer 126 (2018), 504–508.

[31] Nield, D.A. and Bejan, A. Convection in porous media. Fifth Ed., Springer, Cham, Switzerland (2017).

[32] Rees, D.A.S. The effect of inertia on free convection from a horizontal surface embedded in a porous medium. Int. J. Heat Mass Transfer 39 (1996), 3425–3430.

[33] Rees, D.A.S. The effect of inertia on the onset of mixed convection in a porous layer heated from below. Int. Comm. Heat Mass Transfer 24 (1997), 277–283.

[34] Vadasz, P. Coriolis effect on gravity-driven convection in a rotating porous layer heated from below. J. Fluid Mech. 376 (1998), 351–375.

[35] Altawallbeh, A. A., Bhadauria, B. S. and Hashim, I. Linear and nonlinear double - diffusive convection in a saturated anisotropic porous layer with Soret effect and internal heat source. Int. J. Heat Mass Transfer 59 (2013), 103–111.

[36] Bhadauria, B. S. and Srivastava, A.K. Magneto - double diffusive convection in an electrically conducting - fluid - saturated porous medium with temperature modulation of the boundaries. Int. J. Heat Mass Transfer 53 (2010), 2530–2538.

[37] Falsaperla, P., Mulone, G. and Straughan, B. Inertia effects on rotating porous convection. Int. J. Heat and Mass Transfer, 54 (2011), 1352–1359.

[38] Harfash, A.J. and Challoob, H.A. Slip boundary conditions and throughflow effects on double diffusive convection in internally heated heterogeneous Brinkman porous media. Chinese J. Physics 56 (2018), 10–22.

[39] Straughan, B. Structure of the dependence of Darcy and Forchheimer coefficients on porosity. Int. J. Engng. Sci., 48 (2010), 1610–1621.

[40] Straughan, B. Porous convection with Cattaneo heat flux. Int. J. Heat Mass Transfer 53 (2010), 2808–2812.

[41] Straughan, B. Heat Waves, volume 177 of Applied Mathematical Sciences, Springer, New York, 2011.

[42] Nield, D.A. and Kuznetsov, A.V. Forced convection in a bidisperse porous medium channel: conjugate problem. Int. J. Heat Mass Transfer, 47 (2004) 5375-5380.

[43] Nield, D.A. and Kuznetsov, A.V. The effect of combined vertical and horizontal heterogeneity on the onset of convection in a bidisperse porous medium. Int. J. Heat Mass Transfer, 50 (2007) 3329-3339.

[44] Nield, D.A. and Kuznetsov, A.V. Natural convection about a vertical plate embedded in a bidisperse porous medium. Int. J. Heat Mass Transfer, 51 (2008), 1658-1664.

[45] Nield, D.A. and Kuznetsov, A.V. A note on modelling high speed flow in a bidisperse porous medium. Trans. Porous Media, 96 (2013)495-499.

[46] Nield, D.A. A note on the modelling of a bidispersive porous media. Trans. Porous Media, 111 (2016) 517-520.

[47] Falsaperla, P., Mulone, G. and Straughan, B. Bidispersive inclined convection. Proc. Roy. Soc. London A, 472 (2016) 20160480.

[48] Gentile, M. and Straughan, B. Bidispersive thermal convection. Int. J. Heat Mass Transfer, 114 (2017), 837–840.

[49] Franchi, F., Nibbi, R. and Straughan, B. Continuous dependence on modelling for temperature dependent bidispersive flow. Proc. Roy. Soc. London A, 173 (2017), 20170485.

[50] Gentile, M. and Straughan, B. Bidispersive vertical convection. Proc. Roy. Soc. London A, 173 (2017), 20170481.

[51] Straughan, B. Horizontally isotropic bidispersive thermal convection. Proc. Roy. Soc. London A 474 (2018), 20180018.

[52] Chandrasekhar, S. Hydrodynamic and hydromagnetic stability. Dover Publications (1981).

[53] Straughan, B. Importance of Darcy or Brinkman laws upon resonance in thermal convection. Ricerche di Matematica 65 (2016), 349–362.

[54] Straughan, B. Exchange of stability in Cattaneo-LTNE porous convection. Int. J. Heat Mass Transfer, 89 (2015), 792–798.

J	R	R_{stat}	a^2	σ_1^2	C^*
0.1	24.742036	24.733183	9.6833	-0.90545$\times 10^{-3}$	0.910
0.1	24.742185	24.743183	9.6833	0.42789$\times 10^{-3}$	0.920
0.3	25.700209	25.693183	9.3647	0.61709$\times 10^{-3}$	1.870
0.3	25.700516	25.703183	9.3646	0.12537$\times 10^{-2}$	1.880
0.5	26.645475	26.643183	9.1029	0.16002$\times 10^{-2}$	2.820
0.5	26.645971	26.653183	9.1028	0.20153$\times 10^{-2}$	2.830
0.8	28.044546	28.043183	8.7859	0.23282$\times 10^{-2}$	4.220
0.8	28.045320	28.053183	8.7857	0.26000$\times 10^{-2}$	4.230
1.0	28.967200	28.963183	8.6114	0.25957$\times 10^{-2}$	5.140
1.0	28.968149	28.973183	8.6112	0.28164$\times 10^{-2}$	5.150

Table 1: Critical values of R, a^2 and σ_1^2 for quoted values J, at the transition from stationary to oscillatory convection. C^* is the corresponding value of $\mathcal{C}$ at the transition. Values of R_{stat} the stationary convection value are also given. Here, $K_r = 1.5, \xi = 0.1$.

J	R	R_{stat}	a^2	σ_1^2	C^*
0.1	36.103225	36.093615	9.6255	-0.33138$\times 10^{-3}$	1.550
0.1	36.103332	36.103615	9.6255	0.45046$\times 10^{-3}$	1.560
0.3	37.934585	37.933615	9.2183	0.13893$\times 10^{-2}$	3.390
0.3	37.934749	37.943615	9.2183	0.17370$\times 10^{-2}$	3.400
0.5	39.734085	39.733615	8.8919	0.21210$\times 10^{-2}$	5.190
0.5	39.734334	39.743615	8.8919	0.23420$\times 10^{-2}$	5.200
0.8	42.388781	42.383615	8.5048	0.27390$\times 10^{-2}$	7.840
0.8	42.389160	42.393615	8.5047	0.28807$\times 10^{-2}$	7.850
1.0	44.136008	44.133615	8.2951	0.30816$\times 10^{-2}$	9.590
1.0	44.136472	44.143615	8.2950	0.31954$\times 10^{-2}$	9.600

Table 2: Critical values of R, a^2 and σ_1^2 for quoted values J, at the transition from stationary to oscillatory convection. C^* is the corresponding value of $\mathcal{C}$ at the transition. Values of R_{stat} the stationary convection value are also given. Here, $K_r = 5.0, \xi = 0.1$.

J	R	R_{stat}	a^2	σ_1^2	C^*
0.1	25.000933	24.995700	9.7032	-0.49568$\times 10^{-3}$	0.870
0.1	25.001063	25.005700	9.7032	0.90653$\times 10^{-3}$	0.880
0.3	25.862930	25.855700	9.4117	0.45008$\times 10^{-3}$	1.730
0.3	25.863145	25.865700	9.4117	0.11399$\times 10^{-2}$	1.740
0.5	26.713806	26.705700	9.1659	0.11698$\times 10^{-2}$	2.580
0.5	26.714140	26.715700	9.1658	0.16242$\times 10^{-2}$	2.590
0.8	27.973718	27.965700	8.8603	0.19555$\times 10^{-2}$	3.840
0.8	27.974238	27.975700	8.8601	0.22543$\times 10^{-2}$	3.850
1.0	28.804743	28.795700	8.6885	0.22994$\times 10^{-2}$	4.670
1.0	28.805382	28.805700	8.6883	0.25419$\times 10^{-2}$	4.680

Table 3: Critical values of R, a^2 and σ_1^2 for quoted values J, at the transition from stationary to oscillatory convection. C^* is the corresponding value of $\mathcal{C}$ at the transition. Values of R_{stat} the stationary convection value are also given. Here, $K_r = 1.5, \xi = 0.5$.

J	R	R_{stat}	a^2	σ_1^2	C^*
0.1	40.991481	40.988418	9.6848	0.37918$\times 10^{-4}$	1.510
0.1	40.991591	40.998418	9.6848	0.84783$\times 10^{-3}$	1.520
0.3	42.560481	42.598418	9.3627	0.25685$\times 10^{-2}$	3.120
0.3	42.560623	42.608418	9.3627	0.29558$\times 10^{-2}$	3.130
0.5	44.105847	44.098418	9.0924	0.15190$\times 10^{-2}$	4.620
0.5	44.106053	44.108418	9.0924	0.17712$\times 10^{-2}$	4.630
0.8	46.391929	46.388418	8.7576	0.23303$\times 10^{-2}$	6.910
0.8	46.392238	46.398418	8.7576	0.24943$\times 10^{-2}$	6.920
1.0	47.897897	47.888418	8.5700	0.25830$\times 10^{-2}$	8.410
1.0	47.898276	47.898418	8.5699	0.27159$\times 10^{-2}$	8.420

Table 4: Critical values of R, a^2 and σ_1^2 for quoted values J, at the transition from stationary to oscillatory convection. C^* is the corresponding value of $\mathcal{C}$ at the transition. Values of R_{stat} the stationary convection value are also given. Here, $K_r = 5.0, \xi = 0.5$.

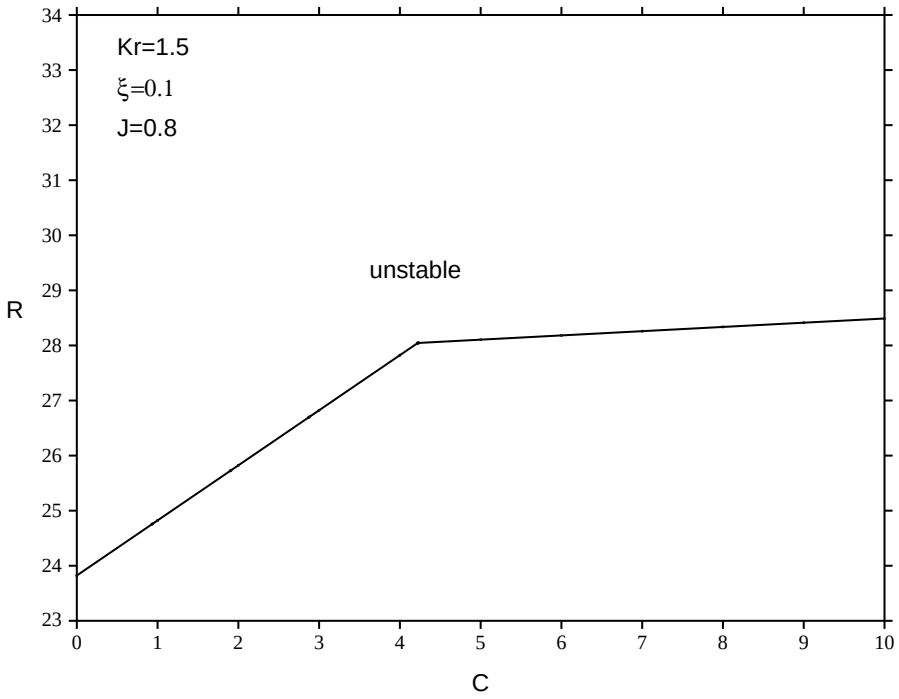

Figure 1: Critical Rayleigh number R against the salt Rayleigh number $\mathcal{C}$. The slanted line beginning with R just below 24 is the stationary convection curve. The other intersecting curve shows where oscillatory convection occurs. Instability occurs for values above the displayed lines. The saturating fluid is water, the porous material is sand, $\phi = 0.3, \epsilon = 0.2$ and $\mathcal{L} = \epsilon_1 Le = 55.924$.

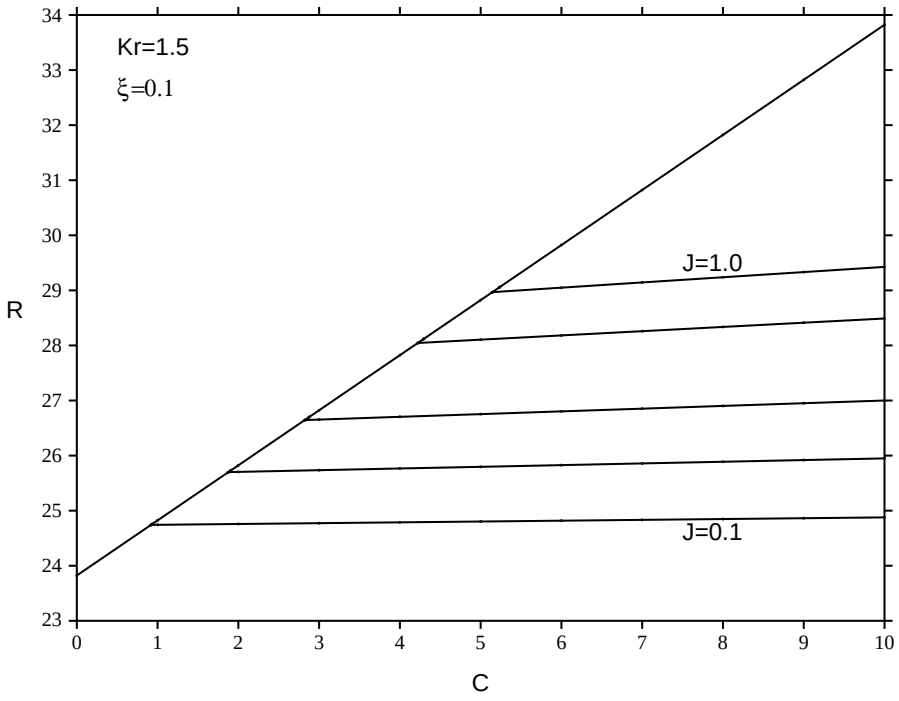

Figure 2: Critical Rayleigh number R against the salt Rayleigh number $\mathcal{C}$. The slanted line beginning with R just below 24 is the stationary convection curve. The other intersecting curves show where oscillatory convection occurs. The oscillatory convection curves are for $J = 0.1$, the lowest, then $J = 0.3, 0.5, 0.8, 1.0$, with R increasing as J does.

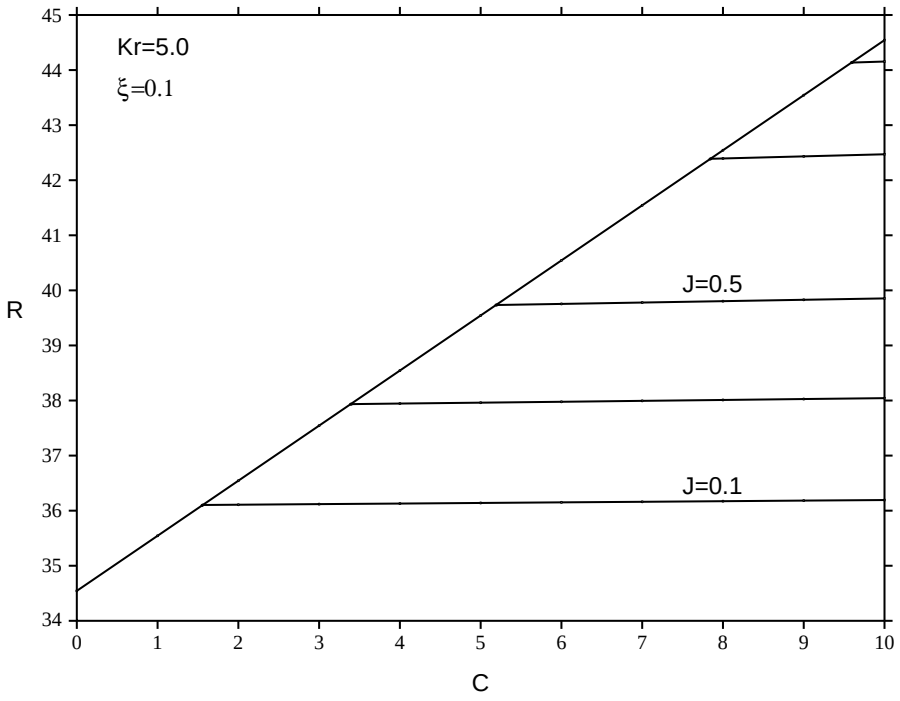

Figure 3: Critical Rayleigh number R against the salt Rayleigh number $\mathcal{C}$. The slanted line beginning with R just above 34 is the stationary convection curve. The other intersecting curves show where oscillatory convection occurs. The oscillatory convection curves are for $J = 0.1$, the lowest, then $J = 0.3, 0.5, 0.8, 1.0$, with R increasing as J does.

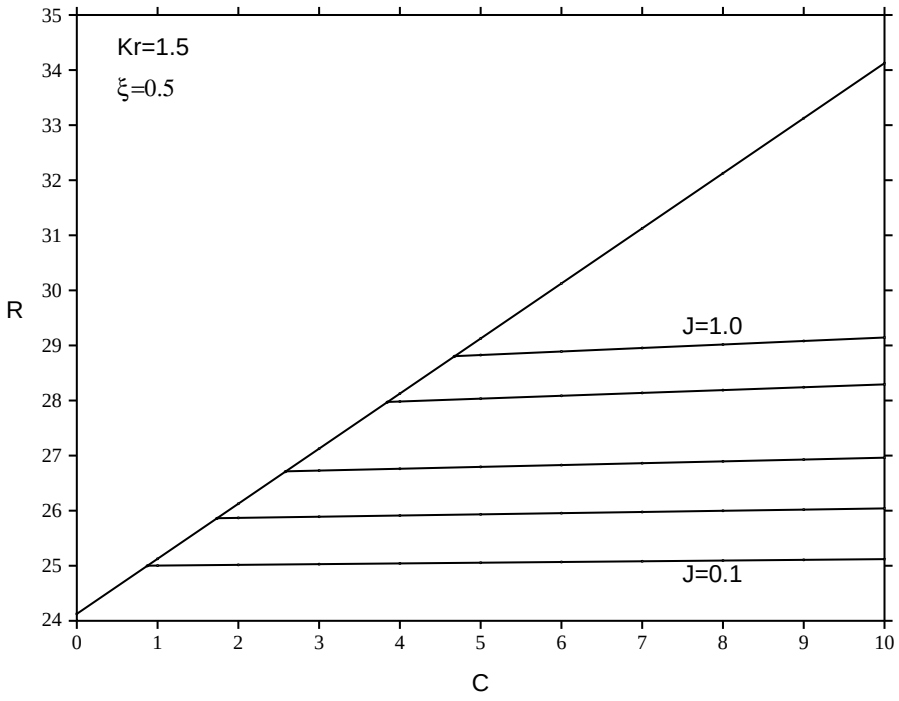

Figure 4: Critical Rayleigh number R against the salt Rayleigh number $\mathcal{C}$. The slanted line beginning with R just above 24 is the stationary convection curve. The other intersecting curves show where oscillatory convection occurs. The oscillatory convection curves are for $J = 0.1$, the lowest, then $J = 0.3, 0.5, 0.8, 1.0$, with R increasing as J does.

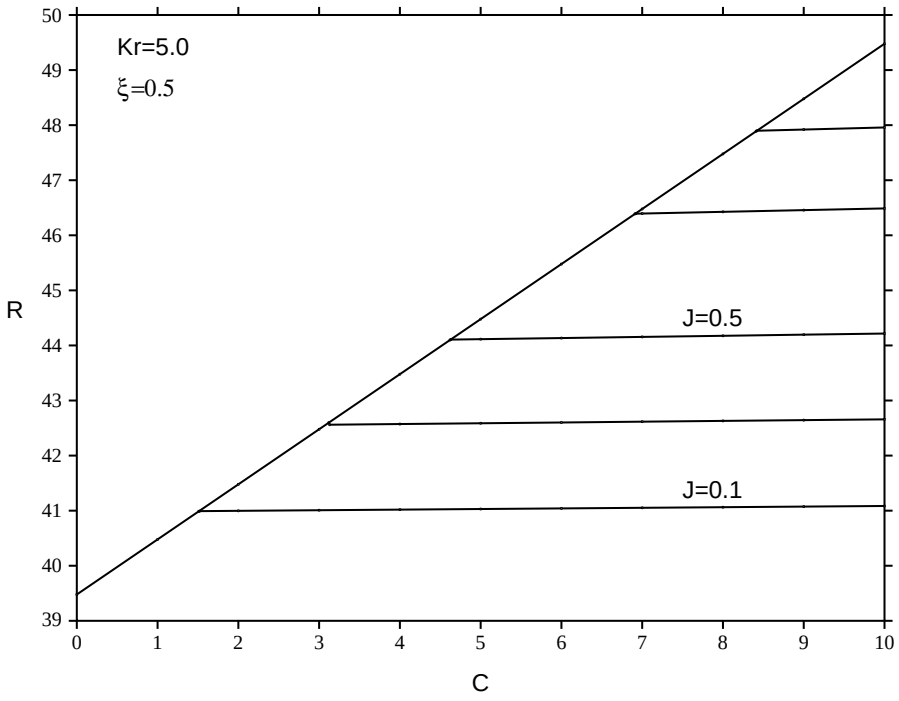

Figure 5: Critical Rayleigh number R against the salt Rayleigh number $\mathcal{C}$. The slanted line beginning with R just above 39 is the stationary convection curve. The other intersecting curves show where oscillatory convection occurs. The oscillatory convection curves are for $J = 0.1$, the lowest, then $J = 0.3, 0.5, 0.8, 1.0$, with R increasing as J does.

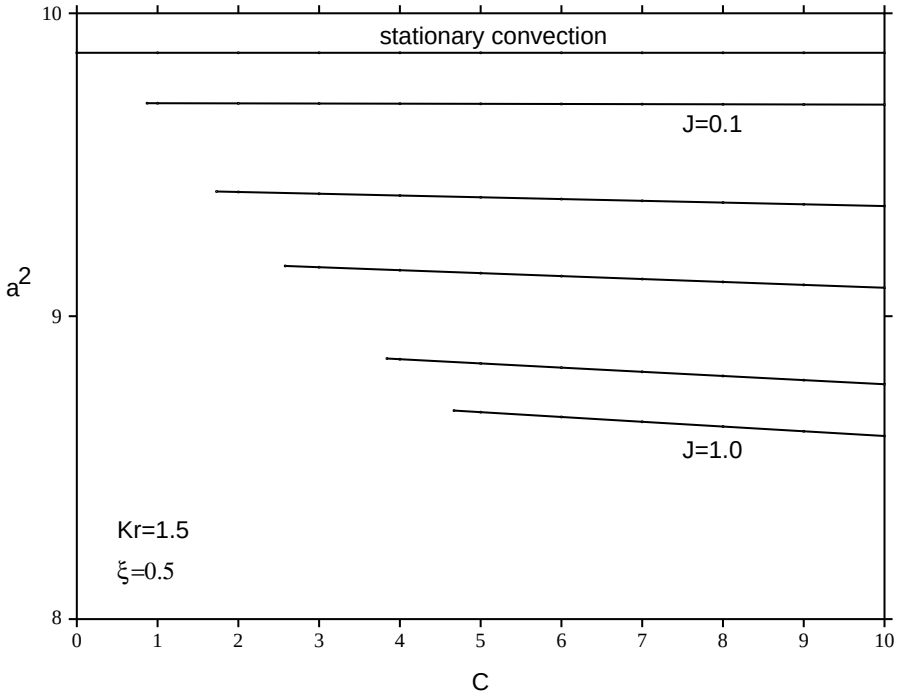

Figure 6: Critical wavenumber squared a^2 against the salt Rayleigh number $\mathcal{C}$. The horizontal line $a^2 = \pi^2 \approx 9.8696$ is the stationary convection curve. The other curves show where oscillatory convection occurs. The oscillatory convection curves are for $J = 1.0$, the lowest, then $J = 0.8, 0.5, 0.3, 0.1$, with a^2 decreasing as $\mathcal{C}$ increases. The oscillatory curves jump from the stationary curve at the transition values $\mathcal{C} = 0.87, J = 0.1, a^2 = 9.7032$; $\mathcal{C} = 1.73, J = 0.3, a^2 = 9.4117$; $\mathcal{C} = 2.58, J = 0.5, a^2 = 9.1659$; $\mathcal{C} = 3.84, J = 0.8, a^2 = 8.8603$; $\mathcal{C} = 4.67, J = 1.0, a^2 = 8.6885$. For completeness the transition Rayleigh number values are (to 3 decimal places) $R = 24.996, J = 0.1$; $R = 25.856, J = 0.3$; $R = 26.710, J = 0.5$; $R = 27.966, J = 0.8$; $R = 28.796, J = 1.0$.